

# Nonlocal continuous-variable quantum nondemolition gates by optical connections

Michele N. Notarnicola<sup>1,\*</sup> and Radim Filip<sup>1,†</sup>

<sup>1</sup>*Department of Optics, Palacký University, 17. Listopadu 12, 779 00 Olomouc (Czech Republic)*

(Dated: March 16, 2026)

Nonlocal quantum gates, coupling quantum systems located at distance, are crucial for distributed quantum computing. High-capacity optical noiseless connections between these quantum systems are essential for transmitting large amounts of information per mode. We propose a library of feasible protocols to implement a necessary nonlocal continuous-variable (CV) quantum nondemolition (QND) gate between two distant users sharing a quantum channel with a newly available element - single-pass phase-sensitive optical parametric amplifiers (OPAs), allowing for both online squeezing and channel-loss compensation, and classical communication between them. The use of OPAs enhances quality of the resulting entangling gate in terms of both excess noise and logarithmic negativity. The proposed schemes are also applicable to CV cluster state fusion, providing a first step towards development of distributed CV measurement-based quantum computation.

## I. INTRODUCTION

Distributed quantum computing [1–4] is a crucial paradigm for the efficient scale up of quantum computers, obtained by mapping qubits to a nonlocal quantum network of smaller processing units, e.g. cluster states [5–7], connected through quantum channels to build larger quantum processors. To this aim, the realization of nonlocal quantum gates that entangle different network nodes represents a fundamental step. Originally proposed in the early 2000s [8–12], those gates allow two distant users sharing a quantum channel, Alice ( $A$ ) and Bob ( $B$ ), to effectively implement a joint unitary operation by means of both local operations and classical communication (LOCC) and the exchange of an ancillary system through the channel to mediate the interaction, hereafter referred to as mediator ( $M$ ). Experimental demonstrations have been only recently realized on discrete-variable (DV) platforms, where a nonlocal controlled-NOT (CNOT) operation has been distributed over distances of 0.6, 7, 10 km, respectively [13–15].

The continuous-variable (CV) analog of the CNOT gate is the quantum nondemolition (QND) coupling  $U_{AB} = \exp(-igx_A p_B/2)$ , where  $g \in \mathbb{R}$  is the gate gain,  $x_j, p_j$ ,  $j = A, B$ , are quadrature operators, namely the position- and momentum-like variables, expressed in shot-noise units and satisfying  $[x_j, p_k] = 2i\delta_{jk}$  [16]. The nondemolition gate is advantageous for CV processing due to its versatility [17]. The input-output transformation in Heisenberg picture reads:

$$\begin{cases} x'_A = x_A, & p'_A = p_A - gp_B, \\ x'_B = x_B + gx_A, & p'_B = p_B, \end{cases} \quad (1)$$

showing  $x_A$  and  $p_B$  as nondemolishing variables, whose information is transmitted to  $x'_B$  and  $p'_A$ , respectively. Local QND interaction is directly available in quantum optomechanics and atomic ensembles [18–22], and its all-optical implementation has also been tested [23, 24]. However, use of online squeezers instead of measurement-induced schemes [12] would be essential for the realization of nonlocal CV gates.

The recent development of single-pass optical parametric amplifiers (OPAs) [25–29] shed new light on this subject. Waveguide-based OPAs are  $\chi^{(2)}$ -fabricated waveguides that perform online squeezing of optical signals throughout propagation, showing higher optical nonlinearities than conventional cavity-based methods [30–32]. As active online elements, they may be employed to both build QND interaction in optics [24] and perform signal restoration as phase-sensitive amplifiers (PSAs) [16, 33–35], offering new possibilities for distributed quantum information.

In this work, we propose a list of different measurement-induced OPA-assisted protocols to distribute essential QND gates at distance, assuming QND (1) is locally available to both the remote users Alice and Bob, and employing mediators that exhibit different quantum resources: squeezing [Fig. 1(a)], entanglement [Fig. 1(b)], Bell measurement [Fig. 1(c)] and the geometric phase effect by sequential local QNDs [Fig. 1(d)]. We characterize the resulting nonlocal entangling gates in terms of both logarithmic negativity and excess noise and optimize their performance, proving the first three schemes to be equivalent with one another, whilst the geometric phase protocol to give a factor 2 improvement over the others in both the limits of small and large losses. Further, we demonstrate application of our approach for fusion of distant cluster states into a distributed network [36]. The structure of the paper is the following. Firstly, in Sec. II we derive a model for realistic OPAs in the presence of losses. Then, in Sec.s III and IV we present the proposed schemes to achieve nonlocal QND and their application for cluster state fusion, respectively. Finally, in Sec. V we draw conclusions.

## II. A MODEL FOR REALISTIC WAVEGUIDE OPAS

Together with online squeezing, a realistic waveguide OPA is expected to have distributed losses occurring throughout propagation along the waveguide, beyond incoupling and out-coupling losses. Accordingly, the optical output state is described by the master equation  $\dot{\rho} = -i[H_{\text{OPA}}, \rho] + \gamma \mathcal{L}[a]\rho$ , where  $H_{\text{OPA}} = i\chi[(a^\dagger)^2 - a^2]/2$  is the squeezing Hamiltonian,  $\chi \in \mathbb{R}$ ,  $\gamma \geq 0$  is the loss rate and  $\mathcal{L}[O]\rho = O\rho O^\dagger - \{O^\dagger O, \rho\}/2$  is the Lindblad operator. An equivalent descrip-

\* michelenicola.notarnicola@upol.cz

† filip@optics.upol.cz

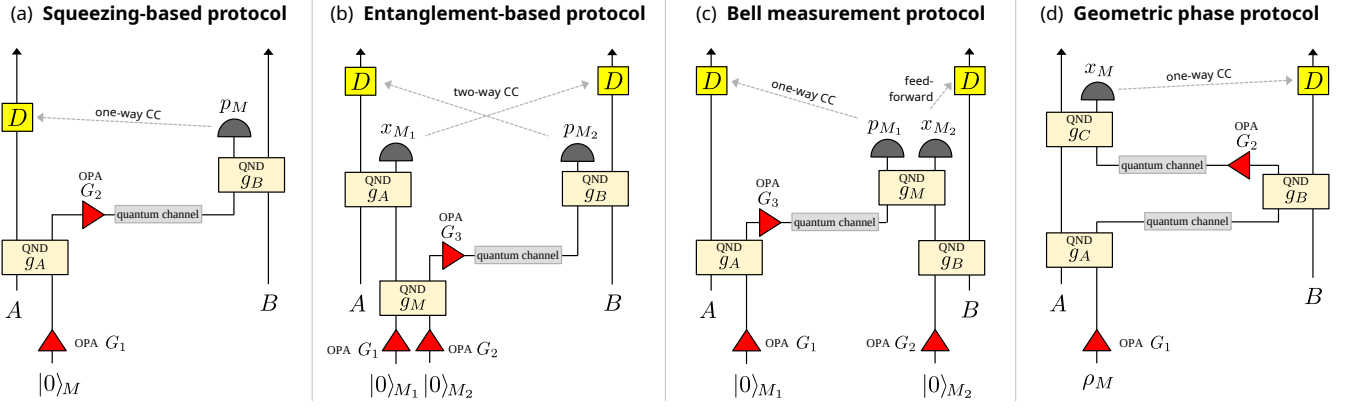


Figure 1. Schemes for nonlocal QND gate implementation. The squeezing-based (SB) protocol (a) uses an offline-squeezed vacuum mediator with single quantum channel and one-way classical communication (CC). The entanglement-based (EB) scheme (b) exploits entanglement pre-sharing, by designing an optimized two-mode state that fits into QNDs  $g_{A(B)}$ , at the cost of two-way CC, while the Bell measurement (BM) one (c) replaces the prior resource distribution with online entanglement generation by QND-based Bell measurement, reducing the classical resources to one-way CC and feed-forward. Unlike the previous setups, the geometric phase (GP) protocol enables nonlocal gates independent of the mediator state, at the costs of double use of quantum channel, large offline squeezing  $G_1 \rightarrow 0$  and one more gate at Alice's side. In all setups, it is also possible to design local Gaussian gates that integrate QNDs together with the OPAs. Displacements might also be done by QND interaction with classical coherent light controlled by the measured results. We assume ideal homodyne detection, for if detectors have low quantum efficiency, one can use a further OPA as pre-amplifier [37].

tion for the quadratures  $x = a + a^\dagger$  and  $p = i(a^\dagger - a)$ , in the Heisenberg picture, derived in App. A, is given in terms of pure squeezing followed by squeezed-thermal-loss channel:

$$x' = \sqrt{\eta G} x + \sqrt{1-\eta} x_n, \quad p' = \sqrt{\frac{\eta}{G}} p + \sqrt{1-\eta} p_n, \quad (2)$$

where:

$$G = e^{2\chi t} > 0 \quad \text{and} \quad \eta = e^{-\gamma} \geq 0 \quad (3)$$

are the amplifier gain and efficiency, respectively,  $t$  being the interaction time fixed by the waveguide length, while  $x_n, p_n$  are quadrature operators of the channel-noise mode, excited in a squeezed thermal state with  $\langle x_n \rangle = \langle p_n \rangle = 0$  and

$$\langle x_n^2 \rangle = \frac{1-\eta G}{1-\eta} \frac{\ln(\eta)}{\ln(\eta G)}, \quad \langle p_n^2 \rangle = \frac{1-\eta/G}{1-\eta} \frac{\ln(\eta)}{\ln(\eta/G)}. \quad (4)$$

For a lossless amplifier  $\eta = 1$ , we retrieve the unitary squeezing transformation  $x' = \sqrt{G}x$  and  $p' = p/\sqrt{G}$ , that amplifies (squeezes) quadrature  $x$  if  $G > 1$  ( $G < 1$ ), whereas in the absence of squeezing,  $G = 1$ , Eq. (2) yields a pure-loss channel. Advantageously, this representation is easy to combine with the incoupling and outcoupling loss to an unified operator transformations. Nevertheless, while coupling losses are described by pure-loss channels, distributed OPA losses introduce external thermal noise in the signal mode, with more crucial impact on realistic applications.

### III. NONLOCAL QND GATES

Fig. 1 schematizes the proposed protocols for distributed gates, where Alice and Bob wish to implement a nonlocal

QND gate with target gain  $g > 0$ . The first minimal scheme, named squeezing-based (SB) protocol [Fig. 1(a)], requires two local gates, and both a single quantum and classical-communication channels [11]. The quantum channel is a pure-loss channel of transmissivity  $T \leq 1$ . We assume Alice to possess an auxiliary vacuum mediator  $M$ , being offline squeezed by an OPA of parameters  $\eta_1, G_1$ , and then coupled to  $A$  by local QND (1) of gain  $g_A > 0$ . Thereafter, Alice transmits  $M$  to Bob, through the pure-loss channel, preceded by a second OPA with  $\eta_2, G_2$ , operating as PSA to pre-compensate for channel losses [16, 33]. Crucially, the PSA should be placed before the channel, so as to amplify only  $M$  and not the additional channel-loss mode. Bob then couples  $M$  to  $B$  by a second QND gate of gain  $g_B = g/(g_A \sqrt{\eta_2 G_2 T})$ , measures quadrature  $p_M$  via homodyne detection and classically communicate the measurement outcome  $\bar{p}$  to Alice, who applies the momentum-like displacement  $p_A \rightarrow p_A + g_A \sqrt{\eta_2 G_2 T} \bar{p}$ .

The second protocol is the entanglement-based (EB) [Fig. 1(b)], where, now, Alice and Bob share an entangled resource state created from two vacuum mediators  $M_{1(2)}$  squeezed by OPAs 1(2) and undergoing local QND of gain  $g_M \equiv -g_0/g_A < 0$ . The resource, located in Alice's lab, can be advantageously priorly distributed between  $A$  and  $B$  through the channel, with OPA 3 acting as PSA, and stored before its use. On their own branch, Alice and Bob implement QNDs of gains  $g_A > 0$  and  $g_B = g/(g_A \sqrt{\eta_3 G_3 T})$ , respectively, followed by homodynes of  $x_{M_1}$  and  $p_{M_2}$ . After two-way classical communication of the outcomes  $\bar{x}, \bar{p}$ , displacements  $p_A \rightarrow p_A + g_0 \sqrt{\eta_3 G_3 T} \bar{p}$  and  $x_B \rightarrow x_B + g \bar{x}/g_A$  are performed. Here, the possibility to pre-share entanglement, being useful for different applications, additionally requires only a two-way communication channel, which can actually be one physical channel used in both directions.

A similar topology is the Bell measurement (BM) scheme [Fig. 1(c)], that replaces the a priori entangled-state distribution of EB with online entanglement generation by QND-based Bell measurement [38] and only one-way CC. Here, Alice and Bob first perform local QNDs of gain  $g_{A(B)} > 0$  with two independent vacuum mediators  $M_{1(2)}$  priorly squeezed by OPAs 1(2), after which  $A$  sends  $M_1$  to  $B$  via the channel, with OPA 3 as PSA. In Bob's lab,  $M_1$  and  $M_2$  are entangled by a Bell measurement, realized by QND of gain  $g_M = -g/(g_A g_B \sqrt{\eta_3 G_3 T}) < 0$  and homodynes of  $p_{M_1}$  and  $x_{M_2}$ . Given the outcomes  $\bar{x}, \bar{p}$ , we finally implement displacements  $p_A \rightarrow p_A + g_A \sqrt{\eta_3 G_3 T} \bar{p}$  and  $x_B \rightarrow x_B - g_B \bar{x}$ , that require one-way CC  $B \rightarrow A$  and feed-forward on Bob's side.

For all these three schemes  $s = \text{SB, EB, BM}$ , the overall modes transformation for  $A, B$  (see App. B for details) is obtained as:

$$\begin{cases} x'_A = x_A, & p'_A = p_A - g p_B + \mathcal{N}_p^{(s)}, \\ x'_B = x_B + g x_A + \mathcal{N}_x^{(s)}, & p'_B = p_B, \end{cases} \quad (5)$$

implementing an additive-Gaussian-noise map that effectively realizes nonlocal unity-gain QND (1) between  $A$  and  $B$  up to additive Gaussian noise modes  $\mathcal{N}_{x(p)}^{(s)}$ , that collect the mediator, channel and OPA noise contributions. We have:

$$\begin{aligned} \mathcal{N}_p^{(\text{SB})} &= -g_A(1 - \eta_2 T) \left( \sqrt{\frac{\eta_1}{G_1}} p_M + \sqrt{1 - \eta_1} p_{n,1} \right) \\ &+ g_A \sqrt{\eta_2 G_2 T} \left( \sqrt{1 - T} p_{\text{ch}} + \sqrt{(1 - \eta_2) T} p_{n,2} \right), \end{aligned} \quad (6a)$$

$$\begin{aligned} \mathcal{N}_x^{(\text{SB})} &= \frac{g}{g_A} \left( \sqrt{\eta_1 G_1} x_M + \sqrt{1 - \eta_1} x_{n,1} \right) \\ &+ \frac{g}{g_A \sqrt{\eta_2 G_2 T}} \left( \sqrt{1 - T} x_{\text{ch}} + \sqrt{(1 - \eta_2) T} x_{n,2} \right), \end{aligned} \quad (6b)$$

for the SB protocol, while for EB and BM:

$$\begin{aligned} \mathcal{N}_p^{(\text{EB})} &= -g_0(1 - \eta_3 T) \left( \sqrt{\frac{\eta_2}{G_2}} p_{M_2} + \sqrt{1 - \eta_2} p_{n,2} \right) \\ &+ g_0 \sqrt{\eta_3 G_3 T} \left( \sqrt{1 - T} p_{\text{ch}} + \sqrt{(1 - \eta_3) T} p_{n,3} \right) \\ &- g_A \left( \sqrt{\frac{\eta_1}{G_1}} p_{M_1} + \sqrt{1 - \eta_1} p_{n,1} \right), \end{aligned} \quad (7a)$$

$$\begin{aligned} \mathcal{N}_x^{(\text{EB})} &= \frac{g}{g_0} \left( \sqrt{\eta_2 G_2} x_{M_2} + \sqrt{1 - \eta_2} x_{n,2} \right) \\ &+ \frac{g}{g_0 \sqrt{\eta_3 G_3 T}} \left( \sqrt{1 - T} x_{\text{ch}} + \sqrt{(1 - \eta_3) T} x_{n,3} \right), \end{aligned} \quad (7b)$$

and

$$\begin{aligned} \mathcal{N}_p^{(\text{BM})} &= -g_A(1 - \eta_3 T) \left( \sqrt{\frac{\eta_1}{G_1}} p_{M_1} + \sqrt{1 - \eta_1} p_{n,1} \right) \\ &+ g_A \sqrt{\eta_3 G_3 T} \left( \sqrt{1 - T} p_{\text{ch}} + \sqrt{(1 - \eta_3) T} p_{n,3} \right) \\ &+ \frac{g}{g_B} \left( \sqrt{\frac{\eta_2}{G_2}} p_{M_2} + \sqrt{1 - \eta_2} p_{n,2} \right), \end{aligned} \quad (8a)$$

$$\begin{aligned} \mathcal{N}_x^{(\text{BM})} &= \frac{g}{g_A} \left( \sqrt{\eta_1 G_1} x_{M_1} + \sqrt{1 - \eta_1} x_{n,1} \right) \\ &+ \frac{g}{g_A \sqrt{\eta_3 G_3 T}} \left( \sqrt{1 - T} x_{\text{ch}} + \sqrt{(1 - \eta_3) T} x_{n,3} \right), \end{aligned} \quad (8b)$$

where  $x_{\text{ch}}, p_{\text{ch}}$  are the channel noise quadratures, assumed in the vacuum. As we can see, the EB protocol in the limits  $g_A \ll 1$  and  $G_1 \gg 1$ , for which  $g_A^2 [\eta_1/G_1 + (1 - \eta_1) \langle p_{n,1}^2 \rangle] \ll 1$ , becomes independent of mediator  $M_1$  and turns out to be equivalent to SB. The same happens for the BM scheme that, when  $g_B, G_2 \gg 1$ , is independent of  $M_2$  as  $[\eta_2/G_2 + (1 - \eta_2) \langle p_{n,2}^2 \rangle]/g_B^2 \ll 1$ , so that all three schemes eventually yield the same performance,  $\mathcal{N}_{x(p)}^{(\text{EB})} \approx \mathcal{N}_{x(p)}^{(\text{BM})} \approx \mathcal{N}_{x(p)}^{(\text{SB})}$ . In turn, in both EB and BM it is crucial to employ QND-based entanglement resource and Bell measurement, both available by online OPAs, while the use of conventional two-mode squeezed vacuum states and beam splitter-based Bell measurement increases the added noise  $\mathcal{N}_{x(p)}$  by one shot-noise unit, leading to an entanglement decay w.r.t. SB [11].

Instead, a different result is provided by the last protocol in Fig. 1(d), named geometric phase (GP), as being inspired on the quantum geometric phase effect [39] observed in quantum transducers [40–44]. It uses a single-mode mediator  $M$  excited in arbitrary quantum state  $\rho_M$  and then squeezed by OPA 1, but, unlike the SB scheme, it requires three gates and two quantum channel uses. First, Alice implements QND of gain  $g_A > 0$  with  $M$ . Then, she transmits  $M$  to Bob, who couples performs QND of gain  $g_B > 0$  and sends it back to Alice, now using OPA 2 as PSA before the second passage into the channel. For completeness, we checked that inserting a further OPA to assist also the first channel does not bring advantage. Finally, Alice implements another QND of gain  $g_C = -g \sqrt{G_2/(\eta_2 T g_B^2)} < 0$ , measures  $x_M$  and communicate the outcome  $\bar{x}$  to Bob, who displaces  $x_B \rightarrow x_B + g_B \Gamma \bar{x}$ , with

$$\Gamma = \frac{g - g_A g_B \sqrt{T}}{-g \sqrt{G_2/(\eta_2 T)} + g_A g_B T \sqrt{\eta_2 G_2}}.$$

The overall gate implements the additive-Gaussian-noise map of Eq. (5) with the noise modes:

$$\begin{aligned} \mathcal{N}_p^{(\text{GP})} &= - \left( g_A - \frac{g \sqrt{T}}{g_B} \right) \left( \sqrt{\frac{\eta_1}{G_1}} p_M + \sqrt{1 - \eta_1} p_{n,1} \right) \\ &+ \frac{g \sqrt{1 - T}}{g_B} \left( p_{\text{ch},1} + \sqrt{\frac{G_2}{\eta_2 T}} p_{\text{ch},2} \right) \\ &+ \frac{g}{g_B} \sqrt{\frac{G_2(1 - \eta_2)}{\eta_2}} p_{n,2}, \end{aligned} \quad (9a)$$

$$\begin{aligned} \mathcal{N}_x^{(\text{GP})} &= g_B \left( 1 + \Gamma \sqrt{\eta_2 G_2 T} \right) \left[ \sqrt{\eta_1 G_1 T} x_M \right. \\ &\quad \left. + \sqrt{(1 - \eta_1) T} x_{n,1} + \sqrt{1 - T} x_{\text{ch},1} \right] \\ &+ g_B \Gamma \left( \sqrt{1 - T} x_{\text{ch},2} + \sqrt{(1 - \eta_2) T} x_{n,2} \right), \end{aligned} \quad (9b)$$

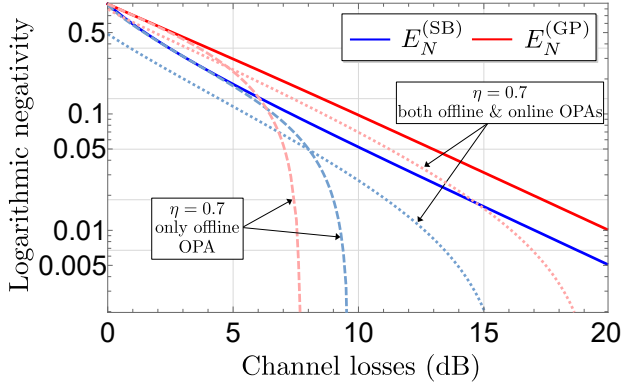


Figure 2. Logarithmic negativity  $E_N^{(s)}$ ,  $s = \text{SB, GP}$ , (solid lines) for target gain  $g = 1$  as a function of the channel losses, equal to  $-10 \log_{10}(T)$  dB. GP scheme outperforms SB, with a factor 2 advantage for  $1 - T \ll 1$ , where  $\partial_T E_N^{(\text{GP})} = \partial_T E_N^{(\text{SB})} / 2$ . Light-colored lines are logarithmic negativities  $E_{N, \text{off(on)}}^{(s)}$  with realistic OPAs ( $\eta = 0.7$ ) for the two cases of only offline squeezing and both online and offline OPAs, that both induce a maximum transmission loss. For  $1 - T \ll 1$ , online OPA is useless for the SB and useful for the GP, provided that  $\eta > \eta_{\text{GP}}(T)$ . The EB and BM protocols are equivalent to the SB.

that, upon choosing

$$g_A = \frac{g\sqrt{T}}{g_B} \quad \text{and} \quad G_1 \rightarrow 0, \quad (10)$$

the latter condition corresponding to large position-like squeezing of  $M$ , become fully independent of the input state  $\rho_M$  of the mediator. Thus, the GP scheme allows for efficient nonlocal QND gates even in the presence of a noisy mediator, e.g. in a highly thermal state [39], at the cost of large offline squeezing and double use of the quantum channel. The impact of finite squeezing  $G_1 > 0$  is discussed in App. B. We also note that the physical principle behind GP is different from the previous protocols, so that even a combination of the schemes in Fig. 1(b) and (c) would yield worse performance.

To assess the quality of the built unity-gain gates (5), we consider as figures of merit (i) the quadrature excess noise  $\xi^{(s)} = \text{Var}[\mathcal{N}_x^{(s)}] = \text{Var}[\mathcal{N}_p^{(s)}]$ ,  $s = \text{SB, EB, BM, GP}$ , in the case of symmetric noise on both Alice and Bob sides, that maximizes the amount of output entanglement and, consequently, (ii) the logarithmic negativity in such case assuming  $A, B$  initially prepared in the vacuum, derived in App. B as:

$$E_N^{(s)} = -\frac{1}{2} \ln \left( 1 + 2g^2 + \xi^{(s)} - 2g\sqrt{1 + g^2 + \xi^{(s)}} \right) \quad (11)$$

for  $\xi^{(s)} < 2g$  and 0 otherwise. The local QND and OPA gains are optimized to minimize (i), thus maximizing (ii). Given that the SB, EB, BM protocols are equivalent with one another, we limit ourselves to compare to the SB and GP schemes, depicted in Fig.s 1(a) and (d), respectively.

For ideal OPAs with  $\eta = 1$ , the optimal configuration for

the SB scheme is obtained by the choices

$$G_1 G_2 = \frac{1 - T}{T} \quad \text{and} \quad g_A = \sqrt{\frac{g G_1}{1 - T}}, \quad (12)$$

for which the excess noise reads  $\xi^{(\text{SB})} = 2g(1 - T)$ . The two OPAs are crucial to protect against the channel losses the information about  $x_A$  to be transferred to Bob, carried by  $x_M$  after the first QND, while that on  $p_B$  is passed to Alice by the final conditional displacement. Remarkably, the maximum entangling power is obtained for finite OPA gains,  $G_1 G_2 < \infty$ , and the corresponding value of  $E_N^{(\text{SB})}$  equals that of the original proposal [11] based on infinite input squeezing and phase-insensitive amplification, thus replacing a non-physical resource with a combination of realistic offline and online squeezers. Consistently with the previous considerations, the EB and BM protocols yields the same performance of the SB in the limits  $g_A^2/G_1 \ll 1$ ,  $G_2 G_3 = (1 - T)/T$ ,  $g_0 = \sqrt{g G_2/(1 - T)}$  (EB) and  $g_B^2 G_2 \gg 1$ ,  $G_1 G_3 = (1 - T)/T$ ,  $g_A = \sqrt{g G_1/(1 - T)}$  (BM).

On the contrary, the GP logarithmic negativity  $E_N^{(\text{GP})}$  is maximized for  $G_2 = T$  and  $g_B = \sqrt{g(1 + T)}$ , together with the mediator-independence conditions (10), leading to  $\xi^{(\text{GP})} = 2g(1 - T)/(1 + T) < \xi^{(\text{SB})}$  and  $E_N^{(\text{GP})} > E_N^{(\text{SB})}$ . Now, OPA 2 perfectly compensates the losses of the second channel on the  $p_M$  quadrature that carries information about  $p_B$  to Alice, at the expense of reducing that on  $x_A$ , which is eventually restored by Bob after displacement. Moreover, the large anti-squeezing noise of  $p_M$  is removed by the last QND gate at Alice's side thanks to the geometric phase trick. As shown in Fig. 2, both SB and GP schemes yield nonzero entanglement for all  $T \leq 1$ . In particular, for small losses  $1 - T \ll 1$ , being of interest for real implementations, we find:

$$E_N^{(s)} \approx E_N^{(0)} - \gamma_s(1 - T), \quad s = \text{SB, GP}, \quad (13)$$

with  $E_N^{(0)}$  computed from (11) with  $\xi = 0$ ,  $\gamma_{\text{SB}} = g(1 - g/\sqrt{1 + g^2})/(1 + 2g^2 - 2g\sqrt{1 + g^2})$  and  $\gamma_{\text{GP}} = \gamma_{\text{SB}}/2$ , whilst in the long-distance regime  $T \ll 1$ ,  $E_N^{(\text{SB})} \approx gT/(1 + g)$  and  $E_N^{(\text{GP})} \approx 2E_N^{(\text{SB})}$ , proving GP to introduce a factor 2 improvement over SB in both the limits.

The scenario changes with realistic OPAs of non-unit efficiency  $\eta < 1$ . As the amplifiers introduce additional losses even in the absence of squeezing, see (2), we identify two different scenarios, case (off): only offline squeezing produced by OPA 1 is considered, while the online PSAs are removed, corresponding to the choices  $\eta_1 = \eta < 1$ ,  $\eta_k = G_k = 1$  for  $k > 1$  in Fig. 1; case (on): we keep all online and offline lossy OPAs with  $\eta_k = \eta < 1$ . The corresponding negativities  $E_{N, \text{off(on)}}^{(s)}(\eta)$ ,  $s = \text{SB, GP}$ , depicted in Fig. 2, exhibit a maximum transmission loss, after which they drop to 0, preventing long-distance entanglement. The entanglement break is a consequence of the thermal noise introduced by the lossy OPAs, that makes the gate excess noise  $\xi_{\text{off(on)}}^{(s)}(\eta)$ , reported in Fig. 3(a), exceed the maximum tolerable threshold  $\xi_{\text{max}} = 2g$

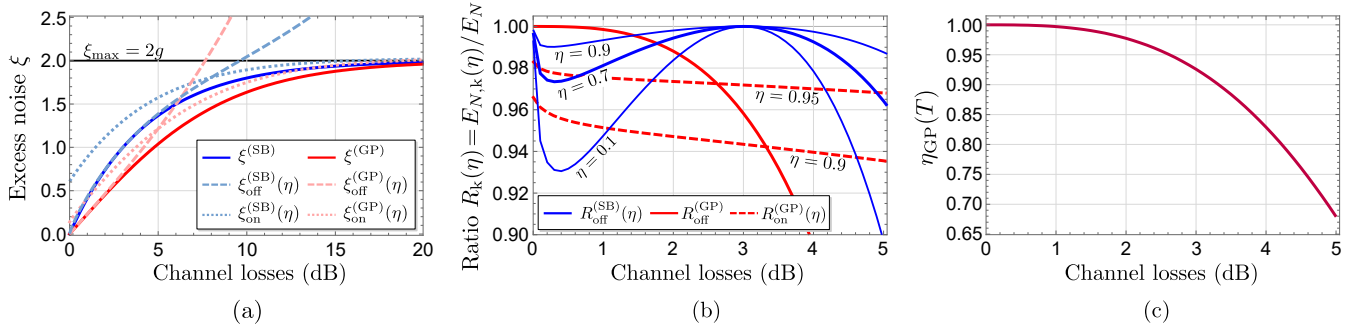


Figure 3. (a) Excess noise  $\xi^{(s)}$ ,  $s = \text{SB}, \text{GP}$ , for target gain  $g = 1$  as a function of the channel losses. For  $1 - T \ll 1$ , GP gives a factor 2 advantage, as  $\xi^{(GP)} = 2g(1 - T)/(1 + T) \approx g(1 - T) = \xi^{(SB)}/2$ . Light-colored lines refer to the cases of lossy OPAs with  $\eta = 0.7$ . Entanglement is lost when  $\xi^{(s)}$  beats the maximum tolerable noise  $\xi_{\max} = 2g$ . (b) Entanglement ratio  $R_k^{(s)} = E_{N,k}^{(s)}(\eta)/E_N^{(s)}$ ,  $k = \text{off}, \text{on}$ , between the realistic case of lossy squeezers and the ideal OPA scheme for  $g = 1$  and different efficiencies  $\eta$ . When  $1 - T \ll 1$ , online OPA is useless for the SB scheme as  $\xi_{\text{on}}^{(SB)}(\eta) > \xi_{\text{off}}^{(SB)}(\eta)$ , whereas, in the GP one, lossy online squeezing helps provided that the OPA efficiency is  $\eta > \eta_{GP}(T)$ . The EB and BM protocols are equivalent to the SB. (c) Threshold OPA efficiency  $\eta_{GP}(T)$  as a function of the channel losses.

for large losses, so that Eq. (11) vanishes. However, when  $T \ll 1$  online OPAs, although being noisy, are still helpful to considerably increase the maximum transmission loss.

Instead, in the opposite limit  $1 - T \ll 1$  the SB and GP schemes behave differently. In the former, the best strategy is to use only OPA 1 as offline squeezer, since for  $1 - \eta \ll 1$  the excess noise in case (off) reads:

$$\xi_{\text{off}}^{(SB)}(\eta) \approx \xi^{(SB)} + g(1 - \eta) \left[ \frac{1 - 2T}{2T \log\left(\frac{1 - T}{T}\right)} - (1 - T) \right], \quad (14)$$

while in case (on) we find  $\xi_{\text{on}}^{(SB)}(\eta) \approx \xi_{\text{off}}^{(SB)}(\eta) + 2g(1 - \eta)$  for both  $1 - \eta, 1 - T \ll 1$ . Therefore, for small channel losses the introduction of online OPA 2, even if slightly lossy, would reduce the gate entangling power, as the amplification gain would be masked by the additional internal losses, whilst it becomes useful in the opposite regime  $T \ll 1$ . The SB output entanglement is also robust to the reduced efficiency, as emerges from the ratios  $R_k^{(s)}(\eta) = E_{N,k}^{(s)}(\eta)/E_N^{(s)}$ ,  $k = \text{off}, \text{on}$ , plotted in Fig. 3(b). In fact,  $R_{\text{off}}^{(SB)}(\eta)$  has a non-monotonic behavior, that for  $1 - T \ll 1$  decreases to a minimum  $\approx 99, 97.3, 93\%$  for  $g = 1$  and  $\eta = 0.9, 0.7, 0.1$ , respectively, and then re-approaches 1 at 3 dB losses, i.e.  $T = 1/2$ , thus showing limited entanglement decay w.r.t. the ideal case. On the other hand, in the GP protocol lossy online OPA 2 is still beneficial, provided its efficiency to be large enough. Indeed, the excess noise for case (off) is independent of  $\eta$ , due to the large offline squeezing  $G_1 \rightarrow 0$ , and equal to:

$$\xi_{\text{off}}^{(GP)} = g \frac{1 - T}{\sqrt{T}} > \xi^{(GP)}, \quad (15)$$

whereas, for  $1 - \eta \ll 1$ ,  $\xi_{\text{on}}^{(GP)}$  is expanded as:

$$\xi_{\text{on}}^{(GP)}(\eta) \approx \xi^{(GP)} + g(1 - \eta) \left[ \frac{T(1 - T)}{(1 + T)^2} - \frac{1 - T}{2 \log T} \right], \quad (16)$$

so that online OPA 2 is helpful if  $\xi_{\text{on}}^{(GP)}(\eta) < \xi_{\text{off}}^{(GP)}$ , namely if  $\eta$  is larger than the threshold function  $\eta_{GP}(T)$  plotted in Fig. 3(c). Correspondingly, the offline entanglement ratio  $R_{\text{off}}^{(GP)}$  is an  $\eta$ -independent monotonic function of  $T$  that rapidly drops from 1, whereas  $R_{\text{on}}^{(GP)}(\eta)$ , albeit being  $< 1$  for  $T = 1$ , is slower decreasing with the channel losses, so that for  $\eta > \eta_{GP}(T)$  it outperforms case (off).

#### IV. CLUSTER STATE FUSION

The nonlocal quantum interaction schemes above demonstrated can be embedded into CV cluster states, namely multi-mode entangled states providing universal resource for measurement-based quantum computation [45–49]. QND clusters may be generated by the quantum circuit in Fig. 4(a), with  $2n$  optical modes  $\{A_k, B_k\}_k$ ,  $k = 1 \dots, n$ , coupled in pairs by two sequences of QNDs (1) of gains  $g_k$  between  $A_k \leftrightarrow B_k$ , and then  $g_{k,k+1}$  between  $B_k \leftrightarrow A_{k+1}$ . The resulting output state is characterized by the set of nullifiers, derived in App. C:

$$\begin{cases} \mathbb{N}_x^{(k)} = x'_{A_{k+1}} - g_{k,k+1} x'_{B_k} = x_{A_{k+1}}, \\ \mathbb{N}_p^{(k)} = p'_{B_k} + g_{k,k+1} p'_{A_{k+1}} = p_{B_k}, \end{cases} \quad (17)$$

where  $\{x_j, p_j\}(\{x'_j, p'_j\})$  are the input (output) quadratures of modes  $j = A_k, B_k$ , for which  $\mathbb{N}_{x(p)}^{(k)} \rightarrow 0$  in the limit of infinite input squeezing,  $\langle x_{A_{k+1}}^2 \rangle = \langle p_{B_k}^2 \rangle = S \rightarrow 0$  [47, 50].

Unlike beam-splitter-based clusters [5, 7], QND entangled states benefit from quantum erasure [51–54], that allows cluster shaping and shortening by homodynes and displacements [55]. Further, here we demonstrate that the nonlocal protocols above presented allow fusion of distinct cluster states [56–58], enabling cluster enlargement at the expense of one (type-I) or two (type-II) qumodes consumption [36]. In particular, the topology depicted in Fig. 4(a) well fits with the EB protocol [see Fig. 1(b)], thus implementing type-II fusion. The BM scheme can be equivalently chosen for the same task, whereas

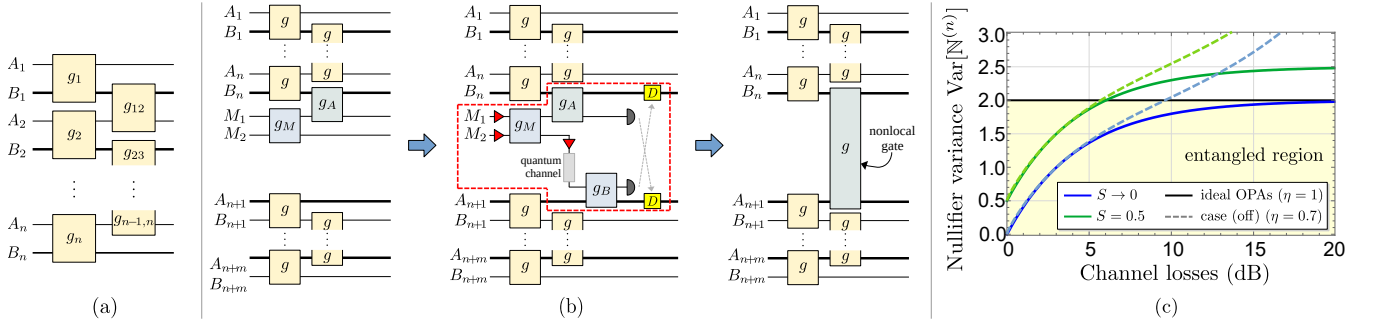


Figure 4. (a) QND-type cluster state of  $2n$  modes. Ideally, this structure may be generated by the setup in [5, 7], based on multiplexing of optical pulses in time-domain, where (passive) beam splitters are replaced with the (active) QND coupling (1). Within the cluster, we distinguish modes that might describe different bosonic systems, e.g mechanical modes or collective spins, (bold line) from those ones considered optical (normal line). (b) Cluster fusion procedure. We consider two distant cluster states of sizes  $2n+2$  between modes  $\{A_1, B_1, \dots, A_n, B_n, M_1, M_2\}$  and  $2m$  between  $\{A_{n+1}, B_{n+1}, \dots, A_{n+m}, B_{n+m}\}$ , respectively. We then send the edge mode  $M_2$  of the first one to the second cluster through an OPA-assisted quantum channel and implement the EB scheme of Fig. 1(b). Eventually, we merge the two local clusters into a single bigger distributed cluster of size  $2(n+m)$ . (c) Nullifier variance  $\text{Var}[\mathbb{N}_{x(p)}^{(n)}] = S + \xi^{(\text{EB})}$  at the edge node  $n$  for different levels of input squeezing  $S$  and gain  $g = 1$ . The entangled region is defined by  $\text{Var}[\mathbb{N}_{x(p)}^{(n)}] < 2g$ . Given the equivalence between EB and SB protocols, for ideal OPAs with  $\eta = 1$ ,  $\text{Var}[\mathbb{N}_{x(p)}^{(n)}] = S + 2g(1 - T)$ , whereas if  $\eta < 1$  online OPA 3 in Fig. 1(b) is useless for  $1 - T \ll 1$ .

SB and GP may be used for type-I fusion of linear cluster states of cascaded QNDs [59].

Let us consider two different QND clusters located at distance, one coupling the  $2n+2$  modes  $\{A_1, B_1, \dots, A_n, B_n, M_1, M_2\}$ , and the other of size  $2m$  between  $\{A_{n+1}, B_{n+1}, \dots, A_{n+m}, B_{n+m}\}$ , as in Fig. 4(b). We fix gains  $g_M = -g_0/g_A < 0$  and  $g_A > 0$  for the gates between  $M_1 \leftrightarrow M_2$  and  $M_1 \leftrightarrow B_n$  [blue boxes in Fig. 4(b)], respectively, while for the other modes  $k = 1, \dots, n+m$  we choose  $g_k = g_{k,k+1} = g$  for simplicity. Given this configuration, if we interpret the last modes of the first cluster as mediators, we recognize the basic topology of the EB protocol. Therefore, we first prepare  $M_{1(2)}$  in two input squeezed states by offline OPAs, then send  $M_2$  through an OPA-assisted quantum channel of transmissivity  $T \leq 1$  to the second cluster, and finally implement QND of gain  $g_B$  with its edge mode  $A_{n+1}$ , followed by homodyne detection and conditional displacements, so that we effectively merge the two distant clusters into a single bigger distributed cluster of size  $2(n+m)$ .

Accordingly, the nullifiers at the edge node  $k = n$  become  $\mathbb{N}_x^{(n)} = x'_{A_{n+1}} - g x'_{B_n} = x_{A_{n+1}} + \mathcal{N}_x^{(\text{EB})}$  and  $\mathbb{N}_p^{(n)} = p'_{B_n} + g p'_{A_{n+1}} = p_{B_n} + \mathcal{N}_p^{(\text{EB})}$ , with the noise operators (7). A sufficient condition for cluster-type entanglement is then provided by the van Loock-Furusawa criterion [60–62]:

$$\text{Var}[\mathbb{N}_x^{(k)}] < 2g \quad \text{and} \quad \text{Var}[\mathbb{N}_p^{(k)}] < 2g, \quad (18)$$

$k = 1, \dots, n+m$  (see App. C), that for  $k \neq n$  implies  $S < 2g$ , with  $S = \langle x_{A_{k+1}}^2 \rangle = \langle p_{B_k}^2 \rangle$ , while at  $k = n$  yields:

$$\text{Var}[\mathbb{N}_{x(p)}^{(n)}] = S + \xi^{(\text{EB})} < 2g, \quad (19)$$

$\xi^{(\text{EB})} = \xi^{(\text{SB})}$  being the nonlocal-gate excess noise plotted in Fig. 3(a), thus determining the maximum tolerable noise

$\xi_{\text{max}} = 2g - S$ . The nullifier variance at the edge node is plotted in Fig. 4(c). For ideal lossless OPAs, where  $\xi^{(\text{EB})} = 2g(1 - T)$ , Eq. (19) conditions the channel transmissivity to  $T > S/2g$ , preventing long-distance multi-mode entanglement for finite input squeezing  $0 < S \leq 1$ .

## V. CONCLUSIONS

We proposed protocols for a nonlocal (distributed) QND gate between two legitimate users that share a quantum channel, over which a mediator exhibiting quantum features, i.e. squeezing, entanglement, geometric phase effect, is exchanged. The users are also endowed with realistic waveguide OPAs, both employed as squeezers and PSAs for channel-loss compensation. We characterized the gate by logarithmic negativity, proving long-distance entanglement for ideal OPAs and robustness to their non-unit efficiency in the small-loss regime. Finally, we showed application of these gates to merge distinct cluster states into a bigger nonlocal one, thus operating cluster fusion gates at distance.

The suggested schemes can be naturally embedded into cluster-state technology, extending the CV fusion strategies firstly proposed in [36] and enabling efficient preparation of large distributed optical networks with different topologies, paving the way for the realization of a global measurement-based CV quantum processor [63, 64]. Moreover, QND interaction may conveniently replace beam splitters as universal two-mode gate for quantum computation, allowing also for efficient synthesis of nonlocal global nonlinear operations by local non-Gaussian cubic phase gates and nonlocal (Gaussian) QNDs [49]. The presented entangling methods are also extendable to other platforms for generation of hybrid entanglement between either CV-CV or DV-CV physical systems mediated by optics [18–22], as well as for quantum transduc-

ers, utilizing a mechanical mediator to couple optical modes not directly interacting [65–68].

### ACKNOWLEDGEMENTS

M.N.N. acknowledges the QuantERA project CLUSSTAR (8C2024003) of the MEYS of the Czech Republic. Project CLUSSTAR has received funding from the EU Horizon Programme under Grant Agreement No. 731473 and 101017733 (QuantERA). R.F. acknowledges the EU Horizon Programme under Grant Agreement No.101080173 (CLUSTEC) and the project CZ.02.01.010022.0080004649 (QUEENTEC) of the EU and the Czech Ministry of Education, Youth and Sport.

### Appendix A: Derivation of the OPA effective model

To derive the Heisenberg representation (2) of realistic OPAs in the presence of distributed losses, we start from the Langevin equations:

$$\begin{cases} \dot{x} = i[H_{\text{OPA}}, x] - \frac{\gamma}{2}x + \sqrt{\gamma}x_{\text{in}}(t), \\ \dot{p} = i[H_{\text{OPA}}, p] - \frac{\gamma}{2}p + \sqrt{\gamma}p_{\text{in}}(t), \end{cases}$$

where  $x, p$  are the quadrature operators of the signal mode traveling through the OPA, expressed in shot-noise units,  $H_{\text{OPA}} = i\chi[(a^\dagger)^2 - a^2]/2 = \chi(xp + px)/4$  is the squeezing Hamiltonian, and  $x_{\text{in}}(t), p_{\text{in}}(t)$  are the time-dependent noisy quadratures of the environment in the input-output formalism [69, 70]. We assume a vacuum bath, such that  $\langle x_{\text{in}}(t) \rangle = \langle p_{\text{in}}(t) \rangle = 0$  and  $\langle x_{\text{in}}(t)x_{\text{in}}(t') \rangle = \langle p_{\text{in}}(t)p_{\text{in}}(t') \rangle = \delta(t-t')$ . Then, after evaluating the commutators we find:

$$\begin{cases} \dot{x} = (\chi - \frac{\gamma}{2})x + \sqrt{\gamma}x_{\text{in}}(t), \\ \dot{p} = -(\chi + \frac{\gamma}{2})p + \sqrt{\gamma}p_{\text{in}}(t), \end{cases}$$

with formal solutions [69]:

$$\begin{aligned} x(t) &= e^{(\chi - \frac{\gamma}{2})t}x(0) + \sqrt{\gamma} \int_0^t dt' e^{(\chi - \frac{\gamma}{2})(t-t')} x_{\text{in}}(t'), \\ p(t) &= e^{-(\chi + \frac{\gamma}{2})t}p(0) + \sqrt{\gamma} \int_0^t dt' e^{-(\chi + \frac{\gamma}{2})(t-t')} p_{\text{in}}(t'), \end{aligned} \quad (\text{A1})$$

where  $t = L/c$  is the interaction time, fixed by the length  $L$  of the waveguide OPA and the light speed  $c$  in the medium. Eq. (A1) yields a Gaussian transformation, therefore it suffices to characterize the output state coming out from the amplifier in terms of its first and second moments. After introducing the notation  $x' = x(t), p' = p(t)$  and  $x = x(0), p = p(0)$  for the output and input signal modes, and the parameters  $G = \exp(2\chi t)$  and  $\eta = \exp(-\gamma t)$ , we find  $\langle x' \rangle = \sqrt{\eta G} \langle x \rangle$ ,

$\langle p' \rangle = \sqrt{\eta/G} \langle p \rangle$ , and

$$\begin{aligned} \langle (x')^2 \rangle &= \eta G \langle x^2 \rangle + \gamma \int_0^t dt' \int_0^t dt'' (\eta G)^{(1 - \frac{t'+t''}{2})} \langle x_{\text{in}}(t') x_{\text{in}}(t'') \rangle \\ &= \eta G \langle x^2 \rangle + \gamma \int_0^t dt' (\eta G)^{(1-t'/t)} \\ &= \eta G \langle x^2 \rangle - \gamma t \frac{1 - \eta G}{\ln(\eta G)} \\ &= \eta G \langle x^2 \rangle + (1 - \eta) \left[ \frac{1 - \eta G}{1 - \eta} \frac{\ln(\eta)}{\ln(\eta G)} \right], \end{aligned} \quad (\text{A2})$$

whilst, similarly,

$$\langle (p')^2 \rangle = \frac{\eta}{G} \langle p^2 \rangle + (1 - \eta) \left[ \frac{1 - \eta/G}{1 - \eta} \frac{\ln(\eta)}{\ln(\eta/G)} \right]. \quad (\text{A3})$$

These results can be interpreted in terms of a mode mixing transformation between a pure-squeezed signal and a (mixed) squeezed thermal state, thus suggesting the effective model in Eq. (2): a sequence of an ideal OPA, performing pure squeezing of gain  $G > 0$ , coupled by a beam splitter of transmissivity  $\eta \leq 1$  to a squeezed-thermal bath state having  $\langle x_{\text{n}} \rangle = \langle p_{\text{n}} \rangle = 0$  and the  $\langle x_{\text{n}}^2 \rangle$  and  $\langle p_{\text{n}}^2 \rangle$  of Eq. (4).

### Appendix B: Extended calculations for the nonlocal QND schemes

We present the extended derivation of the modes linear transformation (5) associated with the discussed nonlocal QND protocols. We start with the SB scheme in Fig. 1(a). First, the mediator  $M$  is squeezed by OPA 1 and coupled to  $A$  by QND of gain  $g_A > 0$ , leading to:

$$\begin{aligned} x_A^{(i)} &= x_A, \quad p_A^{(i)} = p_A - g_A \left( \sqrt{\frac{\eta_1}{G_1}} p_M + \sqrt{1 - \eta_1} p_{n,1} \right), \\ x_M^{(i)} &= \sqrt{\eta_1 G_1} x_M + \sqrt{1 - \eta_1} x_{n,1} + g_A x_A, \quad p_M^{(i)} = p_M. \end{aligned} \quad (\text{B1})$$

Thereafter, Alice transmits  $M$  to Bob through the channel, using OPA 2 for pre-amplification, and Bob performs a second QND of gain  $g_B = g/(g_A \sqrt{\eta_2 G_2 T})$ , obtaining:

$$\begin{aligned} x_M^{(ii)} &= \sqrt{\eta_2 G_2 T} x_M^{(i)} + \sqrt{(1 - \eta_2) T} x_{n,2} + \sqrt{1 - T} x_{\text{ch}}, \\ p_M^{(ii)} &= \sqrt{\frac{\eta_2 T}{G_2}} p_M + \sqrt{(1 - \eta_2) T} p_{n,2} + \sqrt{1 - T} p_{\text{ch}} - g_B p_B, \\ x_B^{(ii)} &= x_B + g_B x_M^{(ii)}, \quad p_B^{(ii)} = p_B. \end{aligned} \quad (\text{B2})$$

Finally, Bob measures  $p_M^{(ii)}$  and communicate the measurement outcome  $\bar{p}$  to Alice, who applies a momentum displacement of amplitude  $g_A \sqrt{\eta_2 G_2 T} \bar{p}$ , that on average implements the Heisenberg transformation  $x_A^{(ii)} = x_A^{(i)}$  and  $p_A^{(ii)} = p_A^{(i)} + g_A \sqrt{\eta_2 G_2 T} p_M^{(ii)}$ . Explicit substitution yields Eq. (6).

With similar method, we approach the EB protocol of Fig. 1(b). We prepare the entangled resource state between

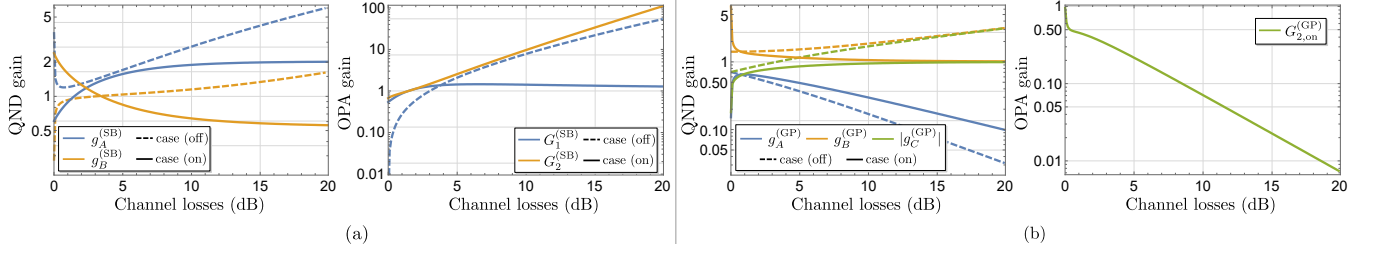


Figure 5. Log plot of the optimized parameters for the SB (a) and GP (b) protocols for target gain  $g = 1$  as a function of the channel losses in cases (off) and (on), respectively, and  $\eta = 0.7$ . In the GP scheme, the optimal configuration of OPA 1 is obtained in the limit  $G_{1,k}^{(GP)} \rightarrow 0$ ,  $k = \text{off, on}$ , corresponding to large position-like squeezing of the mediator  $M$ .

$M_1$  and  $M_2$ , by first squeezing the mediators:

$$\begin{aligned} x_{M_k}^{(i)} &= \sqrt{\eta_k} G_k x_{M_k} + \sqrt{1 - \eta_k} x_{n,k}, \\ p_{M_k}^{(i)} &= \sqrt{\frac{\eta_k}{G_k}} p_{M_k} + \sqrt{1 - \eta_k} p_{n,k}, \quad k = 1, 2, \end{aligned} \quad (\text{B3})$$

and then performing QND of gain  $g_M = -g_0/g_A < 0$ :

$$\begin{aligned} x_{M_1}^{(ii)} &= x_{M_1}^{(i)}, & p_{M_1}^{(ii)} &= p_{M_1}^{(i)} + \frac{g_0}{g_A} p_{M_2}^{(i)}, \\ x_{M_2}^{(ii)} &= x_{M_2}^{(i)} - \frac{g_0}{g_A} x_{M_1}^{(i)}, & p_{M_2}^{(ii)} &= p_{M_2}^{(i)}. \end{aligned} \quad (\text{B4})$$

Subsequently,  $M_2$  is sent through the channel, with OPA 3 as PSA, and Alice and Bob implement QNDs of gain  $g_A > 0$  and  $g_B = g/(g_A \sqrt{\eta_3 G_3 T})$ , so that:

$$\begin{aligned} x_A^{(iii)} &= x_A, & p_A^{(iii)} &= p_A - g_A p_{M_1}^{(ii)}, \\ x_{M_1}^{(iii)} &= x_{M_1}^{(i)} + g_A x_A, & p_{M_1}^{(iii)} &= p_{M_1}^{(ii)} \end{aligned} \quad (\text{B5})$$

and

$$\begin{aligned} x_{M_2}^{(iii)} &= \sqrt{\eta_3 G_3 T} x_{M_2}^{(ii)} + \sqrt{(1 - \eta_3) T} x_{n,3} + \sqrt{1 - T} x_{\text{ch}}, \\ p_{M_2}^{(iii)} &= \sqrt{\frac{\eta_3 T}{G_3}} p_{M_2}^{(i)} + \sqrt{(1 - \eta_3) T} p_{n,3} + \sqrt{1 - T} p_{\text{ch}} - g_B p_B, \\ x_B^{(iii)} &= x_B + g_B x_{M_2}^{(iii)}, & p_B^{(iii)} &= p_B. \end{aligned} \quad (\text{B6})$$

Finally, we measure  $x_{M_1}^{(iii)}$  and  $p_{M_2}^{(iii)}$ , and displace  $p_A^{(iii)}$  and  $x_B^{(iii)}$  to get  $p_A^{(iv)} = p_A^{(iii)} + g_0 \sqrt{\eta_3 G_3 T} p_{M_2}^{(iii)}$  and  $x_B^{(iv)} = x_B^{(iii)} + g x_{M_1}^{(iii)}/g_A$ , leading to (7).

We now move to the BM setup of Fig. 1(c). Like the EB, we first offline squeeze mediators  $M_{1(2)}$  by OPAs 1(2):

$$\begin{aligned} x_{M_k}^{(i)} &= \sqrt{\eta_k} G_k x_{M_k} + \sqrt{1 - \eta_k} x_{n,k}, \\ p_{M_k}^{(i)} &= \sqrt{\frac{\eta_k}{G_k}} p_{M_k} + \sqrt{1 - \eta_k} p_{n,k}, \quad k = 1, 2. \end{aligned} \quad (\text{B7})$$

Thereafter, Alice and Bob performs local QNDs with  $M_{1(2)}$ ,

respectively, such that:

$$\begin{aligned} x_A^{(ii)} &= x_A, & p_A^{(ii)} &= p_A - g_A p_{M_1}^{(i)}, \\ x_{M_1}^{(ii)} &= x_{M_1}^{(i)} + g_A x_A, & p_{M_1}^{(ii)} &= p_{M_1}^{(i)}, \\ x_{M_2}^{(ii)} &= x_{M_2}^{(i)}, & p_{M_2}^{(ii)} &= p_{M_2}^{(i)} - g_B p_B, \\ x_B^{(ii)} &= x_B + g_B x_{M_2}^{(i)}, & p_B^{(ii)} &= p_B. \end{aligned} \quad (\text{B8})$$

Mediator  $M_1$  is then sent to Bob by the OPA-3 assisted channel, and undergoes a Bell measurement with  $M_2$ , consisting of QND of gain  $g_M = -g/(g_A g_B \sqrt{\eta_3 G_3 T}) < 0$ , namely:

$$\begin{aligned} x_{M_1}^{(iii)} &= \sqrt{\eta_3 G_3 T} x_{M_1}^{(ii)} + \sqrt{(1 - \eta_3) T} x_{n,3} + \sqrt{1 - T} x_{\text{ch}}, \\ p_{M_1}^{(iii)} &= \sqrt{\frac{\eta_3 T}{G_3}} p_{M_1}^{(ii)} + \sqrt{(1 - \eta_3) T} p_{n,3} + \sqrt{1 - T} p_{\text{ch}} - g_M p_{M_2}^{(ii)}, \\ x_{M_2}^{(iii)} &= x_{M_2}^{(i)} + g_M x_{M_1}^{(iii)}, & p_{M_2}^{(iii)} &= p_{M_2}^{(i)}, \end{aligned} \quad (\text{B9})$$

followed by homodynes of  $p_{M_1}^{(iii)}$  and  $x_{M_2}^{(iii)}$ . The last operations are the conditional displacements  $p_A^{(iv)} = p_A^{(ii)} + g_A \sqrt{\eta_3 G_3 T} p_{M_1}^{(iii)}$  and  $x_B^{(iv)} = x_B^{(ii)} - g_B x_{M_2}^{(iii)}$ , that give (8).

Instead, in the GP scheme [Fig. 1(d)], we begin by squeezing  $M$  by OPA 1 and performing QND of gain  $g_A > 0$ :

$$\begin{aligned} x_A^{(i)} &= x_A, & p_A^{(i)} &= p_A - g_A \left( \sqrt{\frac{\eta_1}{G_1}} p_M + \sqrt{1 - \eta_1} p_{n,1} \right), \\ x_M^{(i)} &= \sqrt{\eta_1 G_1} x_M + \sqrt{1 - \eta_1} x_{n,1} + g_A x_A, & p_M^{(i)} &= p_M, \end{aligned} \quad (\text{B10})$$

then let the mediator mode pass through the channel for the first time and implement QND with  $B$  of gain  $g_B > 0$ :

$$\begin{aligned} x_M^{(ii)} &= \sqrt{\eta_2 G_2 T} x_M^{(i)} + \sqrt{(1 - \eta_2) T} x_{n,2} + \sqrt{1 - T} x_{\text{ch},1}, \\ p_M^{(ii)} &= \sqrt{\frac{\eta_2 T}{G_2}} p_M + \sqrt{(1 - \eta_2) T} p_{n,2} + \sqrt{1 - T} p_{\text{ch},1} - g_B p_B, \\ x_B^{(ii)} &= x_B + g_B x_M^{(ii)}, & p_B^{(ii)} &= p_B, \end{aligned} \quad (\text{B11})$$

and finally transmit it back to Alice by the second passage

through the channel:

$$\begin{aligned} x_M^{(iii)} &= \sqrt{\eta_3 G_3 T} x_M^{(ii)} + \sqrt{(1-\eta_3)T} x_{n,3} + \sqrt{1-T} x_{ch,2}, \\ p_M^{(iii)} &= \sqrt{\frac{\eta_3 T}{G_3}} p_M^{(ii)} + \sqrt{(1-\eta_3)T} p_{n,3} + \sqrt{1-T} p_{ch,2}. \end{aligned} \quad (\text{B12})$$

Now,  $A$  is coupled to  $M$  by the last QND of gain  $g_C = -g\sqrt{G_3/(\eta_3 T g_B^2)} < 0$ :

$$\begin{aligned} x_A^{(iv)} &= x_A, & p_A^{(iv)} &= p_A^{(i)} - g_C p_M^{(iii)}, \\ x_M^{(iv)} &= x_M^{(iii)} + g_C x_A, & p_M^{(iv)} &= p_M^{(iii)}, \end{aligned} \quad (\text{B13})$$

then we measure  $x_M^{(iv)}$  and displace  $x_B^{(ii)}$  by  $x_B^{(iv)} = x_B^{(ii)} + g_B \Gamma x_M^{(iv)}$ , retrieving (9).

### 1. Logarithmic negativity

In all four cases, we effectively implement the additive-Gaussian-noise map  $\mathbf{r}' = \mathbb{S} \mathbf{r} + \mathbf{N}^{(s)}$ ,  $\mathbf{r} = (x_A, p_A, x_B, p_B)$ , where

$$\mathbb{S} = \begin{pmatrix} 1 & 0 & 0 & 0 \\ 0 & 1 & 0 & -g \\ g & 0 & 1 & 0 \\ 0 & 0 & 0 & 1 \end{pmatrix} \quad (\text{B14})$$

is the symplectic matrix associated with ideal QND (1) and  $\mathbf{N}^{(s)} = (0, \mathcal{N}_p^{(s)}, \mathcal{N}_x^{(s)}, 0)$ ,  $s = \text{SB, EB, BM, GP}$ . As a consequence, if system  $AB$  is initially prepared in a Gaussian state with covariance matrix (CM)  $\sigma_{\text{in}} = ((\mathbf{r}_j \mathbf{r}_k + \mathbf{r}_k \mathbf{r}_j)/2)_{jk}$ , the output bipartite state is still Gaussian with CM:

$$\sigma_{\text{out}} = \mathbb{S} \sigma_{\text{in}} \mathbb{S}^T + \sigma_{\text{n}}^{(s)}, \quad (\text{B15})$$

where:

$$\sigma_{\text{n}}^{(s)} = \begin{pmatrix} 0 & 0 & 0 & 0 \\ 0 & \xi_p^{(s)} & 0 & 0 \\ 0 & 0 & \xi_x^{(s)} & 0 \\ 0 & 0 & 0 & 0 \end{pmatrix} \quad (\text{B16})$$

is the excess noise CM associated with the additional modes, and  $\xi_{p(x)}^{(s)} = \text{Var}[\mathcal{N}_{p(x)}^{(s)}]$ . In particular, for input vacuum states considered in the main text, we have  $\sigma_{\text{in}} = \mathbb{1}_4$  and:

$$\sigma_{\text{out}} = \begin{pmatrix} \sigma_A & \sigma_{AB} \\ \sigma_{AB}^T & \sigma_B \end{pmatrix} = \begin{pmatrix} 1 & 0 & g & 0 \\ 0 & 1+g^2+\xi_p^{(s)} & 0 & -g \\ g & 0 & 1+g^2+\xi_x^{(s)} & 0 \\ 0 & -g & 0 & 1 \end{pmatrix}. \quad (\text{B17})$$

Logarithmic negativity is then computed as  $E_N^{(s)} = \max\{0, -\ln(\tilde{d}_-)\}$ , where [71, 72]:

$$\tilde{d}_- = \sqrt{\frac{\tilde{\Delta} - \sqrt{\tilde{\Delta}^2 - 4 \det(\sigma_{\text{out}})}}{2}} \quad (\text{B18})$$

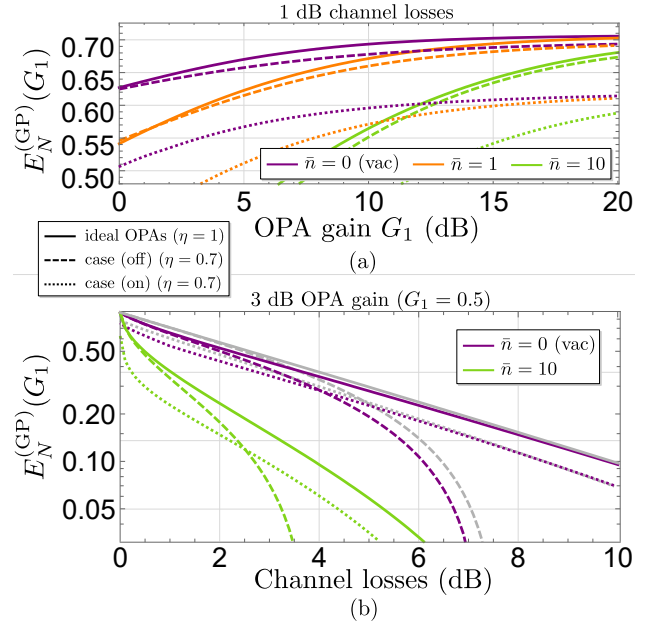


Figure 6. (a) Logarithmic negativity  $E_N^{(GP)}(G_1)$  for target gain  $g = 1$  and 1 dB channel losses as a function of the OPA 1 gain  $G_1$  for different mean thermal photons  $\bar{n}$  of the mediator. For large offline squeezing  $G_1 \ll 1$ , the curves converge to the protocol described in the main text and depicted in Fig. 2. (b) Logarithmic negativity  $E_N^{(GP)}(G_1)$  for target gain  $g = 1$  and fixed OPA 1 gain  $G_1 = 0.5$  (i.e. 3 dB), as a function of the channel losses. The light-gray lines are associated with the protocol of main text and Fig. 2. For vacuum mediator, large OPA 1 gain is needed only for  $1 - T \ll 1$ , while for large losses  $E_N^{(GP)}(G_1)$  approaches the target protocol. On the contrary, with thermal mediator large offline squeezing is crucial in all regimes to both increase negativity for small  $T$  and prevent entanglement break at large  $T$ . In both the figures, solid lines refer to lossless OPAs with unit efficiency, while dashed and dotted ones indicate the performance of realistic OPAs ( $\eta = 0.7$ ) for the two cases of only offline squeezing and both online and offline OPAs, respectively.

is the smallest partially-transposed symplectic eigenvalue, with  $\tilde{\Delta} = I_A + I_B - 2I_{AB}$ ,  $I_k = \det(\sigma_k)$ ,  $k = A, B, AB$ , and is maximized in the symmetric excess noise configuration. In turn, for all the discussed protocols, the local QND and OPA gains are numerically optimized to maximize entanglement (or, equivalently, minimize the excess noise) with the additional constraint  $\xi_p^{(s)} = \xi_x^{(s)} = \xi^{(s)}$ , leading to (11). The optimized parameters for both the SB and GP schemes are discussed in the main text in the case of ideal OPAs, whereas for realistic amplifiers with  $\eta < 1$  we plot them in Fig. 5. The EB protocol is equivalent to SB in the limit  $g_A^2[\eta_1/G_1 + (1-\eta_1/G_1)\ln(\eta_1)/\ln(\eta_1/G_1)] \ll 1$ , while the BM equals SB when  $[\eta_2/G_2 + (1-\eta_2/G_2)\ln(\eta_2)/\ln(\eta_2/G_2)]/g_B^2 \ll 1$ .

### 2. Impact of finite OPA gain in the GP protocol

As discussed in the main text, the GP protocol yields its maximum performance in the limit of large offline squeez-

ing, corresponding to the OPA 1 gain  $G_1 \rightarrow 0$ , see Fig. 1(d). If so, the protocol becomes independent of the mediator, that could be prepared in any arbitrary quantum state  $\rho_M$ . Here, we address robustness of GP to the more realistic scenario of limited offline amplification, namely in the presence of fixed (nonzero) gain  $G_1 > 0$ , where, now, the mediator-independence conditions (10) do not hold and we expect dependence of the scheme on state  $\rho_M$ . To this aim, we consider the mediator in a thermal state  $\rho_M = \sum_{n=0}^{\infty} \bar{n}^n / (\bar{n} + 1)^{n+1} |n\rangle\langle n|$  of  $\bar{n} \geq 0$  average photons, being a typical configuration observed in quantum transducers. Case  $\bar{n} = 0$  then yields the vacuum state  $\rho_M = |0\rangle\langle 0|$ . To qualify the gate, we compute the logarithmic negativity  $E_N^{(\text{GP})}(G_1)$  as a function of both gain  $G_1$  and channel transmissivity  $T$ , by maximizing Eq. (11) over the free parameters  $(g_A, g_B, G_2)$ , with the excess noise (9). As in the main text, we address both the cases of ideal lossless OPAs and lossy amplifiers with efficiency  $\eta < 1$  in cases (off) and (on), corresponding to the use of only offline/both online and offline squeezers, respectively.

$E_N^{(\text{GP})}(G_1)$  is a monotonic function of  $G_1$ , see Fig. 6(a), with asymptotic trend for large enough amplification gain, so that  $E_N^{(\text{GP})}(G_1) \approx E_N^{(\text{GP})}$  for  $G_1 \rightarrow 0$ , with the  $E_N^{(\text{GP})}$  of Fig. 2. Convergence to this regime is faster for a vacuum mediator, while a larger thermal occupancy  $\bar{n} > 0$  requires larger amount of offline squeezing to be compensated. In turn, we observe different behaviors of the logarithmic negativity as a function of the channel losses for fixed gain  $G_1$ , as plotted in Fig. 6(b). With vacuum mediator and ideal OPAs ( $\eta = 1$ ),  $E_N^{(\text{GP})}(G_1)$  is smaller than  $E_N^{(\text{GP})}$  only when  $1 - T \ll 1$ , whilst for  $T \ll 1$ ,  $E_N^{(\text{GP})}(G_1) \approx E_N^{(\text{GP})}$ , proving large offline squeezing to be crucial only in the small loss limit. Analogous considerations hold for lossy OPAs, with  $E_{N,\text{off}}^{(\text{GP})}(G_1) < E_{N,\text{off}}^{(\text{GP})}$ , while  $E_{N,\text{on}}^{(\text{GP})}(G_1) \approx E_{N,\text{on}}^{(\text{GP})}$  for small  $T$ . On the other hand, in the presence of a thermal mediator the logarithmic negativity deviates from the infinite-offline-squeezing protocol for all  $T$ , and for finite squeezing  $G_1 > 0$  it drops to 0 even with lossless OPAs, thus exhibiting a maximum transmission loss that occurs whenever the corresponding excess noise beats the maximum level  $\xi_{\text{max}} = 2g$ . Therefore, in this latter case, a large amplification gain is needed to efficiently distribute entanglement at distance.

### Appendix C: Nullifiers for QND clusters

In this Appendix, we characterize the QND-type cluster state schematized in Fig. 4(a). We first derive the overall quadrature transformation in the Heisenberg picture. Initially, the input modes  $\{A_k, B_k\}_k$ ,  $k = 1, \dots, n$ , undergo a first round of QNDs of gain  $g_k$  between  $A_k$  and  $B_k$ :

$$\begin{aligned} x_{A_k}^{(i)} &= x_{A_k}, & p_{A_k}^{(i)} &= p_{A_k} - g_k p_{B_k}, \\ x_{B_k}^{(i)} &= x_{B_k} + g_k x_{A_k}, & p_{B_k}^{(i)} &= p_{B_k}. \end{aligned} \quad (\text{C1})$$

Then, mode  $B_k$  is further coupled to  $A_{k+1}$  by QND of gain  $g_{k,k+1}$ :

$$\begin{aligned} x_{B_k}^{(\text{ii})} &= x_{B_k}^{(i)}, & p_{B_k}^{(\text{ii})} &= p_{B_k}^{(i)} - g_{k,k+1} p_{A_{k+1}}^{(i)}, \\ x_{A_{k+1}}^{(\text{ii})} &= x_{A_{k+1}}^{(i)} + g_{k,k+1} x_{B_k}^{(i)}, & p_{A_{k+1}}^{(\text{ii})} &= p_{A_{k+1}}^{(i)}, \end{aligned} \quad (\text{C2})$$

leading to the overall transformation:

$$\begin{cases} x'_{A_k} = x_{A_k} + g_{k-1,k} (x_{B_{k-1}} + g_{k-1} x_{A_{k-1}}), \\ p'_{A_k} = p_{A_k} - g_k p_{B_k}, \\ x'_{B_k} = x_{B_k} + g_k x_{A_k}, \\ p'_{B_k} = p_{B_k} - g_{k,k+1} (p_{A_{k+1}} - g_{k+1} p_{B_{k+1}}). \end{cases} \quad (\text{C3})$$

The corresponding nullifiers  $\mathbb{N}_{x(p)}^{(k)}$  are identified by inverting the linear transformation (C3), leading to Eq. (17), so that the cluster state is the zero-eigenvalue eigenstate of  $\mathbb{N}_{x(p)}^{(k)}$  in the limit  $\langle x_{A_{k+1}}^2 \rangle = \langle p_{B_k}^2 \rangle \rightarrow 0$  for all  $k$ , corresponding to infinite input squeezing. In more realistic conditions, a sufficient condition for multi-mode entanglement is derived following the van Loock-Furusawa approach [62] that extends Simon criterion [60], leading to:

$$\text{Var}[\mathbb{N}_x^{(k)}] + \text{Var}[\mathbb{N}_p^{(k)}] < 4|g_{k,k+1}|, \quad (\text{C4})$$

expressed in shot-noise units, that, assuming equal variances  $\text{Var}[\mathbb{N}_x^{(k)}] = \text{Var}[\mathbb{N}_p^{(k)}]$  gives the two independent conditions in Eq. (19).

Finally, in the cluster state fusion procedure of Fig. 4(b), we start with two independent clusters described by transformations (C3) and then implement the EB protocol outlined in App. B. Eventually, we find a single cluster of size  $2(n+m)$ , being still described by transformation (C3) for  $k \neq n, n+1$ , while at the merged nodes  $k = n, n+1$  we now have:

$$\begin{aligned} x'_{A_{n+1}} &= x_{A_{n+1}} + g_{n,n+1} (x_{B_n} + g_n x_{A_n}) + \mathcal{N}_x^{(\text{EB})}, \\ p'_{A_{n+1}} &= p_{A_{n+1}} - g_{n+1} p_{B_{n+1}}, \\ x'_{B_n} &= x_{B_n} + g_n x_{A_n}, \\ p'_{B_n} &= p_{B_n} - g_{n,n+1} (p_{A_{n+1}} - g_{n+1} p_{B_{n+1}}) + \mathcal{N}_p^{(\text{EB})}, \end{aligned} \quad (\text{C5})$$

with the noise operators (7), so that the corresponding nullifiers become  $\mathbb{N}_x^{(n)} = x'_{A_{n+1}} - g_{n,n+1} x'_{B_n} = x_{A_{n+1}} + \mathcal{N}_x^{(\text{EB})}$  and  $\mathbb{N}_p^{(n)} = p'_{B_n} + g_{n,n+1} p'_{A_{n+1}} = p_{B_n} + \mathcal{N}_p^{(\text{EB})}$ .

- [1] J. I. Cirac, A. K. Ekert, S. F. Huelga, and C. Macchiavello, Distributed quantum computation over noisy channels, *Phys. Rev. A* **59**, 4249 (1999).
- [2] L. Jiang, J. M. Taylor, A. S. Sørensen, and M. D. Lukin, Distributed quantum computation based on small quantum registers, *Phys. Rev. A* **76**, 062323 (2007).
- [3] C. Monroe, R. Raussendorf, A. Ruthven, K. R. Brown, P. Maunz, L.-M. Duan, and J. Kim, Large-scale modular quantum-computer architecture with atomic memory and photonic interconnects, *Phys. Rev. A* **89**, 022317 (2014).
- [4] Y. Li and J. D. Thompson, High-rate and high-fidelity modular interconnects between neutral atom quantum processors, *PRX Quantum* **5**, 020363 (2024).
- [5] S. Yokoyama, R. Ukai, S. C. Armstrong, C. Sornphiphatphong, T. Kaji, S. Suzuki, J.-i. Yoshikawa, H. Yonezawa, N. C. Menicucci, and A. Furusawa, Ultra-large-scale continuous-variable cluster states multiplexed in the time domain, *Nat. Photonics* **7**, 982 (2013).
- [6] I. Schwartz, D. Cogan, E. R. Schmidgall, Y. Don, L. Gantz, O. Kenneth, N. H. Lindner, and D. Gershoni, Deterministic generation of a cluster state of entangled photons, *Science* **354**, 434 (2016).
- [7] M. V. Larsen, X. Guo, C. R. Breum, J. S. Neergaard-Nielsen, and U. L. Andersen, Deterministic generation of a two-dimensional cluster state, *Science* **366**, 369 (2019).
- [8] D. Gottesman and I. L. Chuang, Demonstrating the viability of universal quantum computation using teleportation and single-qubit operations, *Nature* **402**, 390 (1999).
- [9] J. Eisert, K. Jacobs, P. Papadopoulos, and M. B. Plenio, Optimal local implementation of nonlocal quantum gates, *Phys. Rev. A* **62**, 052317 (2000).
- [10] M. Paternostro, M. S. Kim, and G. M. Palma, Non-local quantum gates: A cavity-quantum-electrodynamics implementation, *J. Mod. Opt.* **50**, 2075 (2003).
- [11] R. Filip, Continuous-variable quantum nondemolishing interaction at a distance, *Phys. Rev. A* **69**, 052313 (2004).
- [12] R. Filip, P. Marek, and U. L. Andersen, Measurement-induced continuous-variable quantum interactions, *Phys. Rev. A* **71**, 042308 (2005).
- [13] S. Daiss, S. Langenfeld, S. Welte, E. Distante, P. Thomas, L. Hartung, O. Morin, and G. Rempe, A quantum-logic gate between distant quantum-network modules, *Science* **371**, 614 (2021).
- [14] X. Liu, X.-M. Hu, T.-X. Zhu, C. Zhang, Y.-X. Xiao, J.-L. Miao, Z.-W. Ou, P.-Y. Li, B.-H. Liu, Z.-Q. Zhou, et al., Nonlocal photonic quantum gates over 7.0 km, *Nat. Commun.* **15**, 8529 (2024).
- [15] M. Iuliano, N. Demetriou, H. B. van Ommen, C. Karels, T. H. Taminiau, and R. Hanson, Unconditionally teleported quantum gates between remote solid-state qubit registers (2026).
- [16] M. N. Notarnicola, Quantum communications in continuous variable systems, *Int. J. Quantum Inf.* **23**, 2550003 (2025).
- [17] T. Kalajdzievski and N. Quesada, Exact and approximate continuous-variable gate decompositions, *Quantum* **5**, 394 (2021).
- [18] A. Manukhova, A. Rakhubovsky, and R. Filip, Pulsed atom-mechanical quantum non-demolition gate, *npj Quantum Inf.* **6**, 4 (2020).
- [19] R. A. Thomas, M. Parniak, C. Østfeldt, C. B. Møller, C. Bærentsen, Y. Tsaturyan, A. Schliesser, J. Appel, E. Zeuthen, and E. S. Polzik, Entanglement between distant macroscopic mechanical and spin systems, *Nat. Phys.* **17**, 228 (2021).
- [20] A. D. Manukhova, A. A. Rakhubovsky, and R. Filip, Atom-Mechanical Hong-Ou-Mandel Interference, *Quantum* **6**, 686 (2022).
- [21] A. D. Manukhova, A. A. Rakhubovsky, and R. Filip, Nonclassical coincidences of atomic and mechanical excitations, *Phys. Rev. Res.* **6**, 033228 (2024).
- [22] X. Lei, J. Li, X. Zhou, J. Yan, M. Ji, Z. Yan, X. Jia, C. Xie, and K. Peng, Deterministic nonlocal quantum gate with room-temperature memory modules, *Phys. Rev. Lett.* **135**, 130806 (2025).
- [23] S. Yokoyama, R. Ukai, J.-i. Yoshikawa, P. Marek, R. Filip, and A. Furusawa, Nonlocal quantum gate on quantum continuous variables with minimal resources, *Phys. Rev. A* **90**, 012311 (2014).
- [24] Y. Shiozawa, J.-i. Yoshikawa, S. Yokoyama, T. Kaji, K. Makino, T. Serikawa, R. Nakamura, S. Suzuki, S. Yamazaki, W. Asavanant, S. Takeda, P. van Loock, and A. Furusawa, Quantum nondemolition gate operations and measurements in real time on fluctuating signals, *Phys. Rev. A* **98**, 052311 (2018).
- [25] T. Kashiwazaki, K. Enbutsu, T. Kazama, O. Tadanaga, T. Umeki, and R. Kasahara, Over-30-dB phase-sensitive amplification using a fiber-pigtailed PPLN waveguide module, in *Nonlinear Optics (NLO)* (Optica Publishing Group, 2019) p. NW3A.2.
- [26] T. Kashiwazaki, N. Takanashi, T. Yamashita, T. Kazama, K. Enbutsu, R. Kasahara, T. Umeki, and A. Furusawa, Continuous-wave 6-dB-squeezed light with 2.5-thz-bandwidth from single-mode PPLN waveguide, *APL Photonics* **5**, 036104 (2020).
- [27] N. Takanashi, A. Inoue, T. Kashiwazaki, T. Kazama, K. Enbutsu, R. Kasahara, T. Umeki, and A. Furusawa, All-optical phase-sensitive detection for ultra-fast quantum computation, *Opt. Express* **28**, 34916 (2020).
- [28] T. Kashiwazaki, T. Yamashita, N. Takanashi, A. Inoue, T. Umeki, and A. Furusawa, Fabrication of low-loss quasi-single-mode PPLN waveguide and its application to a modularized broadband high-level squeezer, *Appl. Phys. Lett.* **119**, 251104 (2021).
- [29] T. Kashiwazaki, T. Yamashita, K. Enbutsu, T. Kazama, A. Inoue, K. Fukui, M. Endo, T. Umeki, and A. Furusawa, Over-8-dB squeezed light generation by a broadband waveguide optical parametric amplifier toward fault-tolerant ultra-fast quantum computers, *Appl. Phys. Lett.* **122**, 234003 (2023).
- [30] M. N. Notarnicola, M. G. Genoni, S. Cialdi, M. G. A. Paris, and S. Olivares, Phase noise mitigation by a realistic optical parametric oscillator, *J. Opt. Soc. Am. B* **39**, 1059 (2022).
- [31] T. Park, H. Stokowski, V. Ansari, S. Gyger, K. K. S. Multani, O. T. Celik, A. Y. Hwang, D. J. Dean, F. Mayor, T. P. McKenna, M. M. Fejer, and A. Safavi-Naeini, Single-mode squeezed-light generation and tomography with an integrated optical parametric oscillator, *Sci. Adv.* **10**, ead11814 (2024).
- [32] H. S. Stokowski, D. J. Dean, A. Y. Hwang, T. Park, O. T. Celik, T. P. McKenna, M. Jankowski, C. Langrock, V. Ansari, M. M. Fejer, et al., Integrated frequency-modulated optical parametric oscillator, *Nature* **627**, 95 (2024).
- [33] M. N. Notarnicola, F. Ciecich, and M. Jarzyna, Continuous-variable quantum key distribution over multispan links employing phase-insensitive and phase-sensitive amplifiers, *New J. Phys.* **26**, 043015 (2024).

- [34] Z. Yan, H. He, H. Liu, M. Iu, O. Ahmed, E. Chen, P. Blakey, Y. Akasaka, T. Ikeuchi, and A. S. Helmy,  $\chi^2$ -based algaas phase sensitive amplifier with record gain, noise, and sensitivity, *Optica* **9**, 56 (2022).
- [35] P. Zhao, M. Karlsson, and P. A. Andrekson, Low-noise integrated phase-sensitive waveguide parametric amplifiers, *J. Lightwave Technol.* **40**, 128 (2022).
- [36] J. Xin, Qumode fusion for continuous-variable cluster states, *Phys. Rev. A* **108**, 022406 (2023).
- [37] U. Leonhardt and H. Paul, High-accuracy optical homodyne detection with low-efficiency detectors: "preamplification" from antisqueezing, *Phys. Rev. Lett.* **72**, 4086 (1994).
- [38] L. Mišta and R. Filip, Improving teleportation of continuous variables by local operations, *Phys. Rev. A* **71**, 032342 (2005).
- [39] V. Kupčík and R. Filip, Continuous-variable entanglement mediated by a thermal oscillator, *Phys. Rev. A* **92**, 022346 (2015).
- [40] T. Bağcı, A. Simonsen, S. Schmid, L. G. Villanueva, E. Zeuthen, J. Appel, J. M. Taylor, A. Sørensen, K. Usami, A. Schliesser, et al., Optical detection of radio waves through a nanomechanical transducer, *Nature* **507**, 81 (2014).
- [41] A. Jöckel, A. Faber, T. Kampschulte, M. Korppi, M. T. Rakher, and P. Treutlein, Sympathetic cooling of a membrane oscillator in a hybrid mechanical–atomic system, *Nat. Nanotechnol.* **10**, 55 (2015).
- [42] N. Vostrosablin, A. A. Rakhubovsky, and R. Filip, Pulsed quantum continuous-variable optoelectromechanical transducer, *Opt. Express* **25**, 18974 (2017).
- [43] N. Vostrosablin, A. A. Rakhubovsky, U. B. Hoff, U. L. Andersen, and R. Filip, Quantum optomechanical transducer with ultrashort pulses, *New J. Phys.* **20**, 083042 (2018).
- [44] E. Zeuthen, A. Schliesser, A. S. Sørensen, and J. M. Taylor, Figures of merit for quantum transducers, *Quantum Sci. Technol.* **5**, 034009 (2020).
- [45] J. Zhang and S. L. Braunstein, Continuous-variable gaussian analog of cluster states, *Phys. Rev. A* **73**, 032318 (2006).
- [46] P. van Loock, C. Weedbrook, and M. Gu, Building gaussian cluster states by linear optics, *Phys. Rev. A* **76**, 032321 (2007).
- [47] M. Gu, C. Weedbrook, N. C. Menicucci, T. C. Ralph, and P. van Loock, Quantum computing with continuous-variable clusters, *Phys. Rev. A* **79**, 062318 (2009).
- [48] S. Takeda and A. Furusawa, Toward large-scale fault-tolerant universal photonic quantum computing, *APL Photonics* **4**, 060902 (2019).
- [49] N. Budinger, A. Furusawa, and P. van Loock, All-optical quantum computing using cubic phase gates, *Phys. Rev. Res.* **6**, 023332 (2024).
- [50] V. Kala, C. A. Breum, M. V. Larsen, U. L. Andersen, J. S. Neergaard-Nielsen, R. Filip, and P. Marek, Nullifiers of non-gaussian cluster states through homodyne measurement (2025).
- [51] R. Filip, Continuous-variable quantum erasing, *Phys. Rev. A* **67**, 042111 (2003).
- [52] U. L. Andersen, O. Glöckl, S. Lorenz, G. Leuchs, and R. Filip, Experimental demonstration of continuous variable quantum erasing, *Phys. Rev. Lett.* **93**, 100403 (2004).
- [53] F. Buscemi, Channel correction via quantum erasure, *Phys. Rev. Lett.* **99**, 180501 (2007).
- [54] M. Sabuncu, R. Filip, G. Leuchs, and U. L. Andersen, Environment-assisted quantum-information correction for continuous variables, *Phys. Rev. A* **81**, 012325 (2010).
- [55] Y. Miwa, R. Ukai, J.-i. Yoshikawa, R. Filip, P. van Loock, and A. Furusawa, Demonstration of cluster-state shaping and quantum erasure for continuous variables, *Phys. Rev. A* **82**, 032305 (2010).
- [56] F. Verstraete and J. I. Cirac, Valence-bond states for quantum computation, *Phys. Rev. A* **70**, 060302 (2004).
- [57] D. E. Browne and T. Rudolph, Resource-efficient linear optical quantum computation, *Phys. Rev. Lett.* **95**, 010501 (2005).
- [58] N. Rimock, K. Cohen, and Y. Oz, Generalized type-II fusion of cluster states, *Phys. Rev. A* **113**, 012603 (2026).
- [59] J. L. O'Brien, A. Furusawa, and J. Vučković, Photonic quantum technologies, *Nat. Photonics* **3**, 687 (2009).
- [60] R. Simon, Peres-horodecki separability criterion for continuous variable systems, *Phys. Rev. Lett.* **84**, 2726 (2000).
- [61] L.-M. Duan, G. Giedke, J. I. Cirac, and P. Zoller, Inseparability criterion for continuous variable systems, *Phys. Rev. Lett.* **84**, 2722 (2000).
- [62] P. van Loock and A. Furusawa, Detecting genuine multipartite continuous-variable entanglement, *Phys. Rev. A* **67**, 052315 (2003).
- [63] V. Danos, E. D'Hondt, E. Kashefi, and P. Panangaden, Distributed measurement-based quantum computation, *Electron. Notes Theor. Comput. Sci.* **170**, 73 (2007), proceedings of the 3rd International Workshop on Quantum Programming Languages (QPL 2005).
- [64] Y. van Montfort, S. de Bone, and D. Elkouss, Fault-tolerant structures for measurement-based quantum computation on a network, *Quantum* **9**, 1723 (2025).
- [65] N. Lauk, N. Sinclair, S. Barzanjeh, J. P. Covey, M. Saffman, M. Spiropulu, and C. Simon, Perspectives on quantum transduction, *Quantum Sci. Technol.* **5**, 020501 (2020).
- [66] C.-H. Wang, F. Li, and L. Jiang, Quantum capacities of transducers, *Nat. Commun.* **13**, 6698 (2022).
- [67] Y.-B. Hou, X. Ai, R. You, and C. Zhong, Correlated noise can be beneficial to quantum transducers, *Phys. Rev. Res.* **7**, L032042 (2025).
- [68] M. Caleffi, L. d'Avossa, X. Han, and A. Sara Cacciapuoti, Quantum transduction: Enabling quantum networking, *IEEE Commun. Surv. Tutor.* **28**, 4195 (2026).
- [69] A. Serafini, *Quantum Continuous Variables: A Primer of Theoretical Methods* (CRC Press, Boca Raton, 2017).
- [70] M. J. Collett and C. W. Gardiner, Squeezing of intracavity and traveling-wave light fields produced in parametric amplification, *Phys. Rev. A* **30**, 1386 (1984).
- [71] A. Ferraro, S. Olivares, and M. G. A. Paris, *Gaussian states in continuous variable quantum information* (Bibliopolis, Napoli, 2005).
- [72] S. Olivares, Quantum optics in the phase space: A tutorial on gaussian states, *Eur. Phys. J. Special Topics* **203**, 3 (2012).